DYNAMIC STEERING FOR IMPROVED SENSOR AUTONOMY AND CATALOGUE MAINTENANCE

Tyler A. Hobson* and I. Vaughan L. Clarkson
School of Information Technology and Electrical Engineering,
The University of Queensland, Australia

Travis Bessell, Mark Rutten and Neil Gordon
National Security and Intelligence Division,
Defence Science and Technology Group, Australia

ABSTRACT

A number of international agencies endeavour to maintain catalogues of the man-made resident space objects (RSOs) currently orbiting the Earth. Such catalogues are primarily created to anticipate and avoid destructive collisions involving important space assets such as manned missions and active satellites. An agency's ability to achieve this objective is dependent on the accuracy, reliability and timeliness of the information used to update its catalogue.

A primary means for gathering this information is by regularly making direct observations of the tens-of-thousands of currently detectable RSOs via networks of space surveillance sensors. But operational constraints sometimes prevent accurate and timely reacquisition of all known RSOs, which can cause them to become lost to the tracking system. Furthermore, when comprehensive acquisition of new objects does not occur, these objects, in addition to the lost RSOs, result in uncorrelated detections when next observed. Due to the rising number of space-missions and the introduction of newer, more capable space-sensors, the number of uncorrelated targets is at an all-time high. The process of differentiating uncorrelated detections caused by once-acquired now-lost RSOs from newly detected RSOs is a difficult and often labour intensive task. Current methods for overcoming this challenge focus on advancements in orbit propagation and object characterisation to improve prediction accuracy and target identification.

In this paper, we describe a complementary approach that incorporates increased awareness of error and failed observations into the RSO tracking solution. Our methodology employs a technique called dynamic steering to improve the autonomy and capability of a space surveillance network's steerable sensors. By co-situating each sensor with a low-cost high-performance computer, the steerable sensor can quickly and intelligently determine where to steer in order to improve its utility. The sensor-system uses a dedicated parallel-processing architecture to enable it to compute a high-fidelity estimate of the target's prior state error distribution in real-time. Negative information, such as when an RSO is targeted for observation but it is not observed, is incorporated to improve the likelihood of reacquiring the target when attempting to observe the target in future. The sensor is consequently capable of improving its utility by planning each observation using a sensor steering solution that is informed by all prior attempts at observing the target.

We describe the practical implementation of a single experimental sensor and offer the results of recent field measurements and simulations. The proposed approach is applied to the task of Initial Orbit Determination (IOD). By first developing and incorporating a constrained admissible region (CAR), the system is capable of reacquiring an RSO months after it was briefly observed and in spite of the apparent lack of tracking information. The system consequently offers a means of enhancing surveillance for Space Situational Awareness (SSA) via increased system capacity, a higher degree of autonomy and the ability to reacquire objects whose dynamics are insufficiently modelled to cue a conventional space surveillance system for observation and tracking.

1. INTRODUCTION

Destructive collisions of objects in orbit about the Earth threaten the economic viability of space-faring, national security and safety-of-flight of manned space missions [1]. In order to prevent collisions in orbit, a number of international agencies maintain catalogues of as many man-made resident space objects (RSOs) as possible. Such catalogues are used to improve Space Situational Awareness (SAA) permitting the holistic prediction and planning necessary to prevent collisions. The utility and reliability of these catalogues is dependent on the accuracy and timeliness of the information used to maintain them [1]. A crucial source of this information is the regular and direct observation of the tens-of-thousands of RSOs that are currently detectable to these agency's networks of space surveillance sensors. But operational constraints to sensor availability, dynamical modelling and tracking methodologies, can occasionally prevent accurate and timely orbit determination of new detections and reacquisition of catalogued RSOs. Consequently, in spite of an agency's best efforts, RSOs can become lost to the tracking

Figure 1: A GEO survey involving Optus C1, Optus D3 and two unanticipated detections.

system [1–3]. Further compounding this problem, lost RSOs reappear as uncorrelated detections when they are next observed. The process of differentiating uncorrelated detections caused by once-acquired now-lost RSOs from newly detected RSOs is a difficult and often labour intensive task. Due to the rising number of space-missions and the introduction of newer, more capable space-sensors [4], the number of uncorrelated targets (UCTs) is at an all-time high [1]. Current methods for overcoming this challenge focus on advancements in orbit propagation and object characterisation to improve prediction accuracy and target identification [3, 5, 6].

We propose that the occurrence of lost RSOs can be reduced via a complementary approach that involves enabling a tracking system to record and respond to failed observation through high-fidelity state error modelling and improved sensor autonomy. Specifically designed for this purpose, the authors from The University of Queensland (UQ) have previously demonstrated a technique called dynamic steering [7–9]. The technique involves co-situating a low-cost high-performance computer with a steerable space surveillance sensor. The resulting system uses a dedicated parallel-processing architecture to enable it to compute a high-fidelity estimate of the target's prior state error distribution in real-time. Use of a high-fidelity distribution permits the incorporation of negative information [10, 11] — such as when an object is scheduled for observation but is not found within the sensor's Field of View (FOV) — into the distribution, enabling a limited search capability. The steerable sensor consequently has the ability to quickly and intelligently determine where to steer in order to improve the likelihood of reacquiring targets during subsequent observations.

In this paper, we offer the details and preliminary results of a collaborative study, between Defence Science and Technology Group (DST Group) — formerly DSTO — and UQ, concerning the application of dynamic steering to Initial Orbit Determination (IOD). We propose that dynamic steering may be of use in situations similar to the example shown in Fig. 1, which displays a single sidereal-stare directed at a region of the geosynchronous (GEO) belt. In this particular frame, two satellites, Optus C1 and D3, were anticipated. However four objects, appearing as streaks, are observed. Such images are common products of surveillance strategies involving scans of the sky [12] and routine target reacquisition. Retrospectively identifying and reacquiring UCTs can be challenging, as the information that can be gained about the UCTs' trajectory is limited. Whilst specialised hardware and processing techniques involving a constrained admissible region (CAR) have been proposed for such cases [6, 13], there remains a strong reliance on fast response or obtaining many observations. These methods aim to increase confidence whilst measuring, often indirectly, six orbital parameters to a level of accuracy sufficient to cue other sensors in the network. We propose that a combination of dynamic steering and the capturing of *a priori* constraints and assumptions to formulate a CAR, may be a useful means of reacquiring and tracking UCTs when as few as one or two images are available and a relatively long period has elapsed since they were observed.

Section 2 presents a brief review of dynamic steering. A process for generating a plausible state error distribution

via a CAR is proposed in Section 3. Details regarding the experimental system currently employed by DST Group and UQ is detailed in Section 4. Section 5 presents some preliminary data regarding recent field measurements and simulated trials. A concluding discussion is presented in Section 6.

2. REVIEW OF DYNAMIC STEERING

The technique known as dynamic steering has recently been presented and demonstrated by the authors from UQ [7–9]. Dynamic steering was devised as a means of improving the utility of a space surveillance network's steerable sensors, particularly those featuring a relatively constrained FOV. Their utility is improved by enabling these sensors to track and, when required, record and exploit negative information to improve the likelihood of finding a target in future observations.

Dynamic steering is implemented via an augmented Bayesian filtering process. As shown in Fig. 2, a sensor-steering and observation evaluation step are inserted in between a conventional Bayesian filter's time update, observation and measurement update steps. Incorporating these additional elements achieves a feedback loop that combines sensor control and tracking into a single solution, capable of reacting to the outcome of an observation in real time.

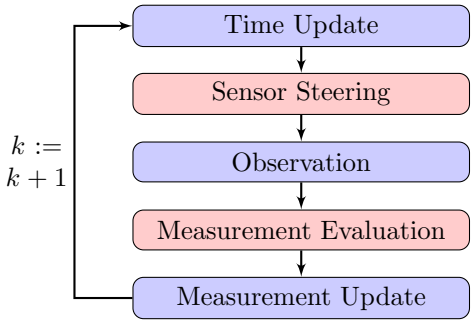

Figure 2: The Bayesian sequential update process with additional (red) steps for dynamic steering.

2.1 Sensor Steering

The role of the sensor steering step is to determine where to point the sensor based on the prior distribution produced during the preceding Bayesian time update. If $\mathbf{x}_k$ is the state of the target at time k and $\mathbf{z}_{1:k-1}$ is the set of all *attempted* observations of the target up until time k, the prior is described by the probability density $p(\mathbf{x}_k|\mathbf{z}_{1:k-1})$.

There are a number of alternative strategies that may be devised to steer the sensor. The question of how to optimally steer the sensor according to the prior remains unresolved. However employing a greedy maximum weight steering strategy, of aiming the sensor in the direction that gains the maximum probability of detection, has thus far demonstrated the greatest potential in the most test cases [9].

To describe the maximum weight sensor steering process, we begin by defining the sensor aiming vector $\mathbf{\Psi}$. This vector contains at least the sensor pointing angles, such as right-ascension α and declination δ, but may also include sensor-specific characteristics such as cost metrics for sensor slewing, unobservable elevations and gimbal-lock limits. An objective function $J(\mathbf{\Psi})$ may be used to evaluate the aiming parameters that achieve the maximum utility, by locating the global maxima. Presuming the sensor's FOV is known but undisclosed, an objective function for obtaining pointing angles with the greatest probability of detection may be described by the equation

$$\mathbf{J}(\mathbf{\Psi}) = \int_{\chi} \mathcal{I}(\mathrm{FOV}(\mathbf{\Psi}))p(\mathbf{x}_k \mid \mathbf{z}_{k-1})\, d\mathbf{x}, \tag{1}$$

where $\mathcal{I}$ is an indicator function defined by

$$\mathcal{I}(\mathrm{FOV}(\mathbf{\Psi})) = \begin{cases} 1 & \mathbf{x} \in \mathrm{FOV}(\mathbf{\Psi}) \\ 0 & \text{otherwise} \end{cases}, \tag{2}$$

χ is the state space and $\mathrm{FOV}(\mathbf{\Psi})$ is the volume, within state space, that is directly or indirectly observable by the sensor's FOV when steered according to $\mathbf{\Psi}$.

2.2 Observation Evaluation

Once the sensor is steered and an observation of the target attempted, the role of the observation evaluation step is to analyse the observation immediately and account for the uncertainty in the outcome, prior to the measurement update. To achieve this task, the observation evaluation step considers traditional measurement data in addition to observation performance metrics. These metrics may include signal-to-noise ratio, data association confidence and environmental considerations such as inclement weather. The ultimate aim is to calculate the probability of detecting the target when it is in the FOV, p_{D}, the probability of falsely detecting the target when the target is not in the FOV, p_{FA} and apply these values appropriately within the measurement update.

Standard Bayesian filtering [14, 15] uses the following equation to implement a measurement update

$$p(\mathbf{x}_k \mid \mathbf{z}_{1:k}) = \frac{p(\mathbf{z}_k \mid \mathbf{x}_k)p(\mathbf{x}_k \mid \mathbf{z}_{1:k-1})}{p(\mathbf{z}_k \mid \mathbf{z}_{1:k-1})}. \tag{3}$$

The observation evaluation step augments this process by incorporating negative information into the likelihood $p(\mathbf{z}_k \mid \mathbf{x}_k)$. We begin by denoting an unsuccessful observation — when a target is scheduled for observation but it is not observed within the FOV — with the parameter $\boldsymbol{\varepsilon}$, which we include as an additional dimension to the measurement vector. Consequently, $\mathbf{z}_k \in \mathbb{R}^{n_{\mathbf{z}}+1}$ where $n_{\mathbf{z}}$ is the number of measurements returned by a sensor and the $(n_{\mathbf{z}}+1)$th element, $\mathbf{z}_{k,n_{\mathbf{z}}+1}$, contains a boolean value such that

$$\mathbf{z}_{k,n_{\mathbf{z}}+1} = \begin{cases} 1 & \text{when target detected in FOV, } [\mathbf{z}_{k,1}, \ldots, \mathbf{z}_{k,n_{\mathbf{z}}}]^{\mathrm{T}} \in \mathbb{R}^{n_{\mathbf{z}}} \\ 0 & \text{when target } \textit{not} \text{ detected in FOV, } \mathbf{z}_k = \boldsymbol{\varepsilon} = \mathbf{0}. \end{cases} \tag{4}$$

The likelihood $p(\mathbf{z}_k \mid \mathbf{x}_k)$ thereafter incorporates this event and the observation evaluation information via the equation

$$p(\mathbf{z}_k \mid \mathbf{x}_k) = \begin{cases} \delta^{n_{\mathbf{z}}+1}(\mathbf{z}_k)(1-p_{\mathrm{D}}) + \delta(\mathbf{z}_{k,n_{\mathbf{z}}+1}-1)p_{\mathrm{D}}p_{\mathrm{Z}}(\mathbf{z}_k \mid \mathbf{x}_k, \boldsymbol{\Psi}_k) & \mathbf{x} \in \mathrm{FOV}(\boldsymbol{\Psi}_k) \\ \delta^{n_{\mathbf{z}}+1}(\mathbf{z}_k)(1-p_{\mathrm{FA}}) + \delta(\mathbf{z}_{k,n_{\mathbf{z}}+1}-1)p_{\mathrm{FA}}p_{\mathrm{U}}(\mathbf{z}_k \mid \boldsymbol{\Psi}_k) & \mathbf{x} \notin \mathrm{FOV}(\boldsymbol{\Psi}_k) \end{cases}. \tag{5}$$

where $\delta^n(\cdot)$ denotes an n-dimensional Dirac delta function. The distribution $p_{\mathrm{Z}}(\mathbf{z}_k \mid \mathbf{x}_k, \boldsymbol{\Psi}_k)$ describes the measurement error characteristics of the sensor and may incorporate the probability of data misassociation. $p_{\mathrm{U}}(\mathbf{z}_k \mid \boldsymbol{\Psi}_k)$ describes the assumed uniform distribution across the FOV in the event of a false alarm. The result is thus a mixed discrete/continuous distribution that depends on the FOV, the presence or absence of a measurement and the reliability of the sensor.

2.3 The Iterative Result

By incorporating the sensor steering and measurement evaluation components within the filtering process, the system can, in real time, determine how to refine the aim of the sensor with each observation attempt. To illustrate this process, Fig. 3 demonstrates the use of the maximum weight objective function (1) to find an elusive RSO. The iteration of the modified Bayesian process results in the convergence of the sensor's bore-sight with the target.

If the target is observed, the system will continue steering the sensor toward the target, enabling further refinement of the target's track. If the target is lost again, the system will seamlessly readopt its search behaviour and autonomously reacquire the target during future observations.

3. CONSTRAINED IOD VIA DYNAMIC STEERING

Dynamic steering permits a relaxation of the traditional constraints imposed upon the collation of targeting information — particularly concerning the level of uncertainty — for cueing conventional surveillance sensors [8, 9]. So long as the target's state error distribution can be represented in high-fidelity by a sensor controller, an autonomous reacquisition can be attempted. We consequently believe that the application of this capability to problems such as reacquiring UCTs using as few as one or two images warrants investigation. Our approach presumes that sensor-RSO relative angles and angle-rates are the only measurements that may be obtained from the available imagery. Thus, we are unable to describe the requisite [13] six-dimensional state error distribution necessary for IOD, due to a lack of information pertaining to range and range-rate. Rather than measure, we infer the missing information by constraining the possible values using a uniform distribution that is bounded by an appropriate CAR (constrained admissible region).

We presume the sensor measurement model $p(\dot{\mathbf{z}}|\dot{\mathbf{z}}_0)$ is known at time $k = 0$, where $\dot{\mathbf{z}}_0$ is a vector containing, for example, measurements of topocentric right ascension, α_{T}, topocentric declination, δ_{T}, and their rates, $\dot{\alpha}_{\mathrm{T}}$ & $\dot{\delta}_{\mathrm{T}}$. To obtain an appropriate CAR, for inferring a distribution of range, ρ, and range-rate, $\dot{\rho}$, a method proposed by DeMars et al. [13, 16] is employed. The method bounds the possible range and range-rate parameters according to constraints

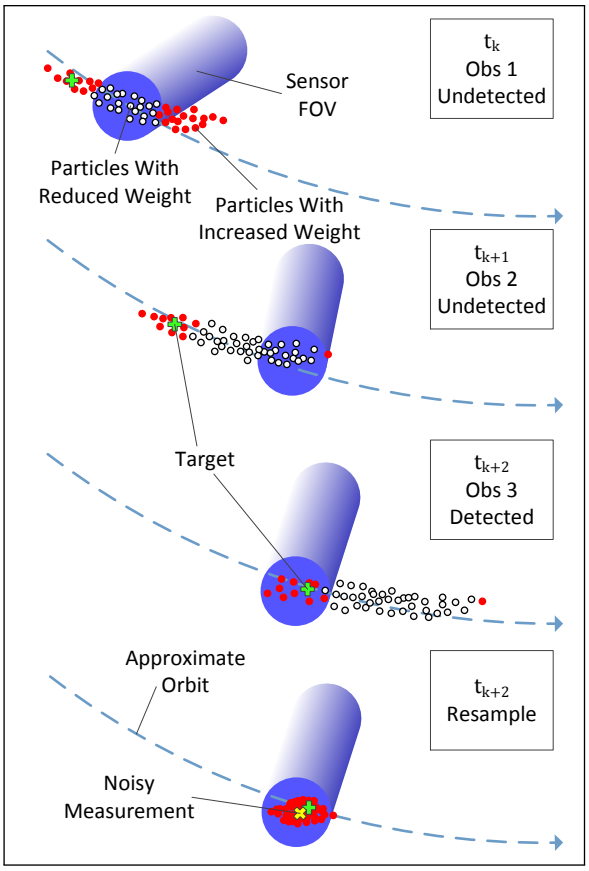

Figure 3: An illustration of a reacquisition achieved using the maximum weight steering strategy. The prior is represented by weighted particles.

to an object's feasible position, $\mathbf{r}$, and velocity, $\dot{\mathbf{r}}$. These constraints are formulated in terms of an object's specific mechanical energy, $\mathcal{E}$, described by

$$\mathcal{E} = \frac{\|\dot{\mathbf{r}}\|^2}{2} - \frac{\mu_\oplus}{\|\mathbf{r}\|} \tag{6}$$

and eccentricity, e, described by

$$e = \sqrt{1 + \frac{2\mathcal{E}\|\mathbf{h}\|^2}{\mu_\oplus^2}} \tag{7}$$

where $\mu_\oplus$ is the Earth's gravitational parameter and $\mathbf{h} = \mathbf{r} \times \dot{\mathbf{r}}$ is the object's specific angular momentum vector. As depicted in Fig. 4, these equations can be rearranged to form a relationship between range and range-rate, provided constraints to an orbit's semi-major axis length, a [13], and eccentricity [16]. The specifics regarding the sensor-RSO geometry necessary for generating Fig. 4 are discussed further in Section 5.

The density $p(\grave{\mathbf{z}}|\grave{\mathbf{z}}_0)$ and an assumed uniform distribution across the CAR may thereafter be combined to describe the six-dimensional distribution $p(\mathbf{z}|\grave{\mathbf{z}}_0, a_1 < a < a_2, e_1 < e < e_2)$, based on the constraints $a_1 < a < a_2$ and $e_1 < e < e_2$. The distribution $p(\mathbf{z}|\grave{\mathbf{z}}_0, a_1 < a < a_2, e_1 < e < e_2) = p(\mathbf{z}|\mathbf{z}_0)$ can be subsequently transformed via an appropriate measurement model, $\mathbf{x} = \mathbf{h}(\mathbf{z})$, to obtain the desired prior $p(\mathbf{x}|\mathbf{z}_0)$.

4. THE EXPERIMENTAL SYSTEM

DST Group is currently developing a research facility for collaborative SSA experimentation. A robotic electro-optical sensor belonging to this facility, located in Edinburgh, South Australia, has been augmented with a dynamic steering capability in a collaborative effort between DST Group and UQ. The system architecture of the experimental sensor is displayed in Fig. 5. The system is composed of two primary elements, a dome to mount and house the electro-optical equipment and a PC to control the robotic telescope and implement dynamic steering.

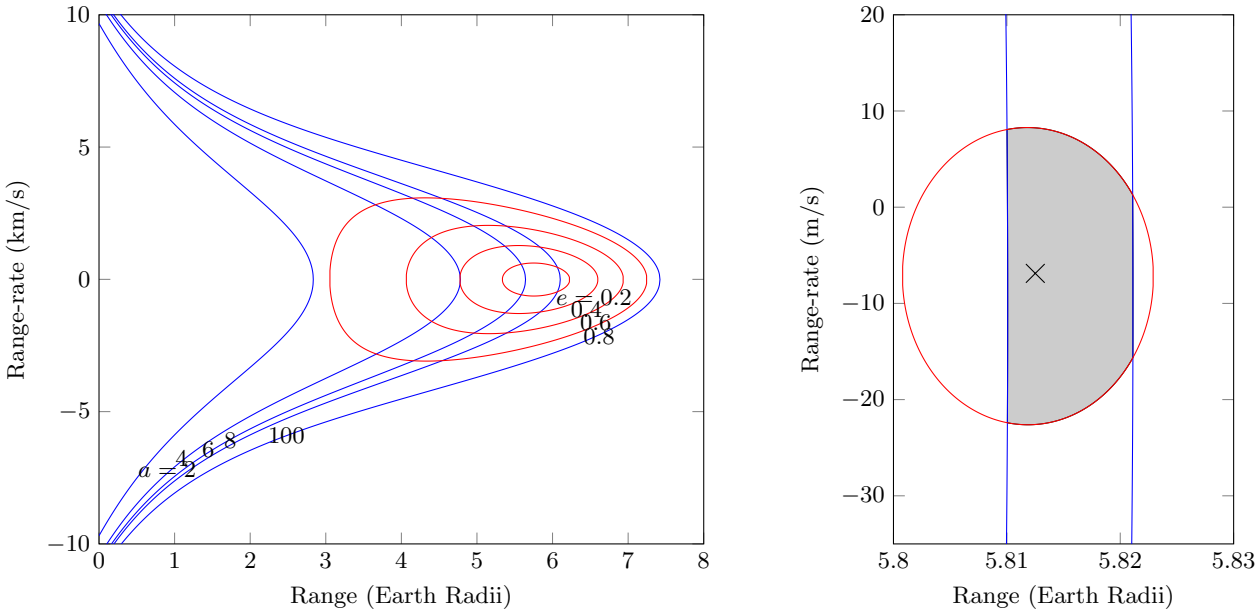

Figure 4: The constrained admissible region (CAR). The plot on the left shows the CAR for several values (Earth radii) of the semi-major axis, a, in blue and eccentricity, e in red. The plot on the right shows the CAR with semi-major axis between 42.10×10^6 m and 42.4×10^6 m (blue lines) and eccentricity between zero and 5×10^{-3} (red ellipse). The grey-shaded area is the resulting admissible region and the true range and range-rate of the object is shown by the cross.

The dome, a 7 ft Aphelion Domes Clamshell, houses three crucial pieces of hardware. An Officina Stellare RH200 telescope is mounted atop a Software Bisque Paramount MEII robotic-mount, and attached to the telescope is an FLI Proline PL4710 camera. The PC, located outside of the dome, is used to operate the camera and robotic mount. These devices are commanded using a program made by Software Bisque, called TheSkyX Pro. TheSkyX Pro obtains precise timing information from a Symmetricom (now Microsemi) GPS timing card. An additional program by Software Bisque named Orchestrate, is used to schedule and initiate multiple observations via TheSkyX Pro. Combined, these COTS elements are capable of autonomously targeting a list of predefined targets and recording time-stamped imagery returned by the sensor. It is the addition of an NVIDIA GTX-980 graphics card, DST Group's in-house astrometry software and a program named Space Particle Search Evaluation (SPARSE) [9] that provide the processing power and feedback-control necessary to implement dynamic steering.

4.1 Astrometry Software

DST Group's astrometry software correlates star catalogues with stars that have been captured in the imagery taken by the electro-optical sensor. The software can map each of the image's pixels to a specific right-ascension and declination, to within approximately an arcsecond of standard deviation. Object detection is thereafter implemented in one of two ways. A rate-tracking method may be used to follow a target with a known trajectory and integrate its light, ideally, on a single pixel. This process causes the stars to streak and the target to appear as a bright dot – see Fig. 6. Alternatively, the software can process sidereal-stare imagery, in which the stars appear to be points and objects streak relative to a starfield background, as has been previously shown in Fig. 1.

Besides accurate angular measurements, use of astrometry also offers a number of outputs that are key to achieving effective observation evaluation for dynamic steering. Notably, the software also returns information about the number of objects in the FOV, a qualitative assessment of occlusion by weather and the precise borsesight angles of the sensor. For experimental purposes only, the astrometry program also offers a high degree of confidence in data association when a recent TLE of the target is supplied. Combined, these metrics are the experimental system's observation performance parameters, that are used during the observation evaluation step.

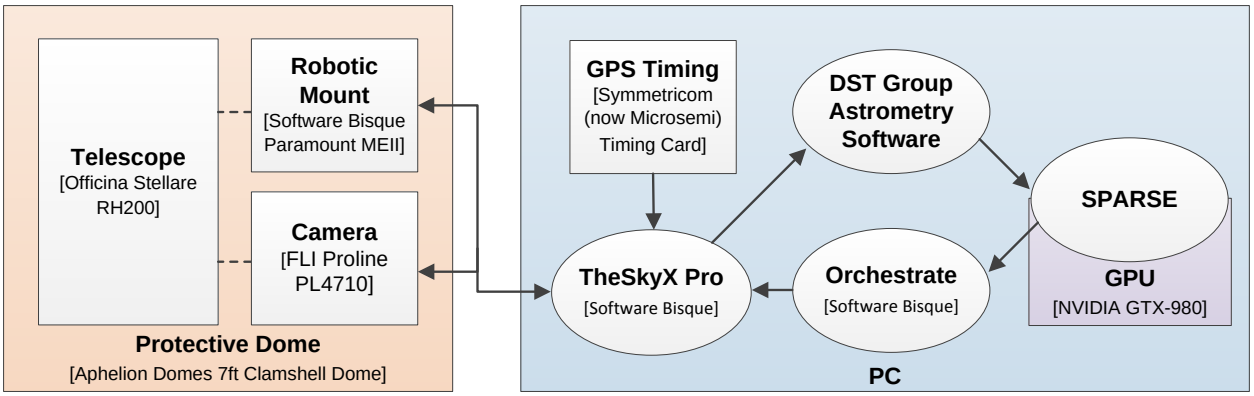

Figure 5: System architecture of the experimental system.

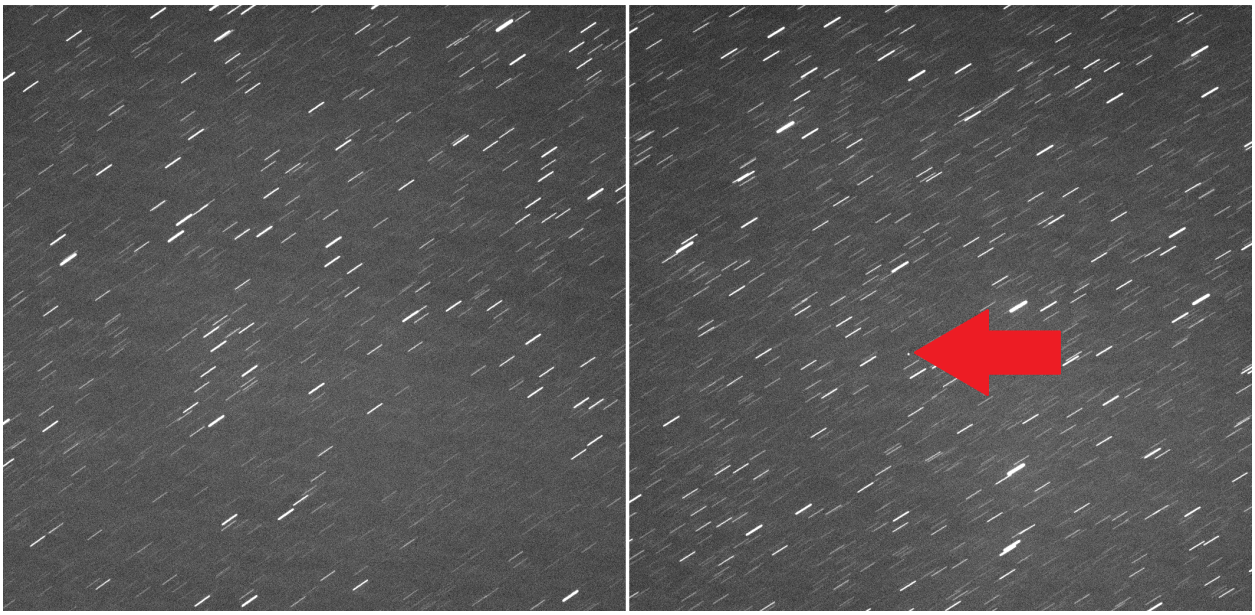

Figure 6: Imagery captured by the DST Group sensor of an RSO outside and within the FOV. Due to rate tracking, the RSO appears as a single dot (indicated by the arrow) and the stars appear as streaks.

4.2 SPARSE

The dynamic steering technique described in Section 2 has been practically implemented in a computer program named SPARSE [9]. The Bayesian filtering process cannot be implemented in closed form, except in some special cases [15] that are not applicable to our application. In place of a pure Bayesian formulation, SPARSE implements dynamic steering via the use of a regularised particle filter (RPF) [9]. Use of an RPF is not a rigorous requirement of practical dynamic steering. Indeed, any number of alternative filtering techniques may be employed, so long as the filter can represent state error densities with sufficient fidelity to capture the highly non-linear propagation of RSO's orbital parameters and negative information – which routinely produces non-Gaussian, often multi-modal, distributions. To accomplish the level of computation required for processing the filter's particle-based representation of the state error distribution, SPARSE utilises a Graphics Processing Unit (GPU) on the experimental system's graphics card [17] to efficiently compute independent processes in parallel.

To enable SPARSE to monitor and control the sensor throughout the dynamic steering process, it employs a range of physical models including planetary motion, planetary orientation, lunar motion, solar illumination, orbit propagation and sensor operation. These models enable SPARSE to monitor observability constraints, propagate the RPF's particles and anticipate the sensor's ability to detect an object at various pointing angles.

As the primary control software, SPARSE initiates observations by sending commands to the sensor via the camera

and mount-control software to initiate rate-tracking observations. The resulting imagery is processed immediately by the DST Group astrometry software. Once evaluated, the observation and performance parameters are passed on to SPARSE to update the distribution and, if required, start the process over again.

5. SYSTEM TRIALS

A series of verification tests using the experimental system were conducted during field trials on 15th April 2015 and again on the 10th June 2015, to ensure dynamic steering had been successfully implemented on the DST Group sensor. Immediately after the success of these trials, imagery was collected to obtain simulated and experimental verification of the proposed IOD method. The Beidou G1 satellite — US Catalogue ID: 36287 — was chosen as the test target. Beidou G1 is routinely visible to Edinburgh and precision orbital data is available to guarantee data association during this initial investigation. Beidou G1 was imaged from Edinburgh using the sidereal stare method on 11th June 2015 at 10:52 UTC.

Whilst using a single image to obtain all measurements will be a case for future investigation, for this study, angular measurements were obtained from a single image while two consecutive images were used to obtain angular rate measurements. The distance between the midpoints of the streaks resulting from the satellite's relative motion were used to obtain a locally linearised angular rate and the measurement error was estimated via a Two-point Differencing method [18]. Using the Beidou G1 imagery, measurement error standard deviations of 2 arcseconds for angular measurements and 8.2×10^{-3} arcseconds per second for their rates were estimated.

Unfortunately, subsequent verification of the imagery indicated that the measurements contained systematic errors and were inappropriate for testing purposes. Furthermore, due to subsequent cloud cover and operational constraints, new observations could not be obtained for this paper. Nevertheless, the measurement error values are believed to be achievable by the system, once the systematic errors are eliminated and new imagery is obtained. The remainder of the section therefore details a simulated verification using equivalent simulated measurements and the measurement error values identified in the trial.

A Beidou G1 two line element (TLE), published on 10th June 2015, was obtained to generate truth data for the simulation. Topocentric angles and rates relative to Edinburgh were computed from the TLE. Gaussian error was added to simulate an appropriately noisy measurement and obtain $p(\grave{\mathbf{z}}|\grave{\mathbf{z}}_0)$. To generate the prior necessary to initiate dynamic steering, the process detailed in Section 3 was implemented by firstly sampling $p(\grave{\mathbf{z}}|\grave{\mathbf{z}}_0)$ to obtain angles and angle-rates. Thereafter the applicable CAR was computed and uniformly sampled to obtain a range and range-rate. The plot on the left of Fig. 4 displays the constant e and a contours that are produced when a sensor, located in Edinburgh, observes the Beidou G1 satellite on 11th June 2015 at 10:53 UTC. The plot on the right shows a more representative CAR for the purposes of initial orbit determination, where the eccentricity and semi-major axis have been constrained to orbits in near-GEO. The near-GEO constraints chosen for this study are displayed in Table 1. The resulting six-dimensional samples were subsequently transformed into SPARSE's preferred state-space, SDP4 elements [19], to achieve a particle representation of the prior $p(\mathbf{x}|\mathbf{z}_0)$.

Table 1: Constraints used to define a GEO-like constrained admissible region.

Parameter	Constraint
semi-major axis length	$42102627 < a < 42384255$ m
eccentricity	$0 < e < 0.05$

To evaluate the experimental system's ability to reacquire Beidou G1 using the CAR-generated distribution, SPARSE was configured to simulate a reacquisition of the target using the attributes of the experimental sensor. Fig. 7 displays a visualisation produced by SPARSE, when performing its first observation attempt, for example, three days after the simulated image was taken. Fig. 7 displays an elongated distribution of 50 000 red particles, due to three days propagation of uncertainty. Beidou G1's location within the distribution is indicated by an orange vector, of inconsequential length, passing from the sensor site and out through the satellite. The simulated sensor's 76 arcminute FOV can be seen targeting the distribution by means of (1). As SPARSE did not capture Beidou G1 within the sensor's FOV, during this observation attempt, the particles within the FOV have been blackened to indicate a reduction in weight. SPARSE thereafter continued searching the distribution for Beidou G1 until the FOV coincided with the satellite.

To test the proposed method's utility for reacquiring targets using aged imagery, the time between the simulated imaging of the satellite and the first attempt to reacquire the satellite was varied from 1 to 88 days. In each case, SPARSE was configured to locate and track the target using the maximum weight steering method. The number of observations required to achieve reacquisition of Beidou G1 was recorded. Fig. 8 displays the results of these

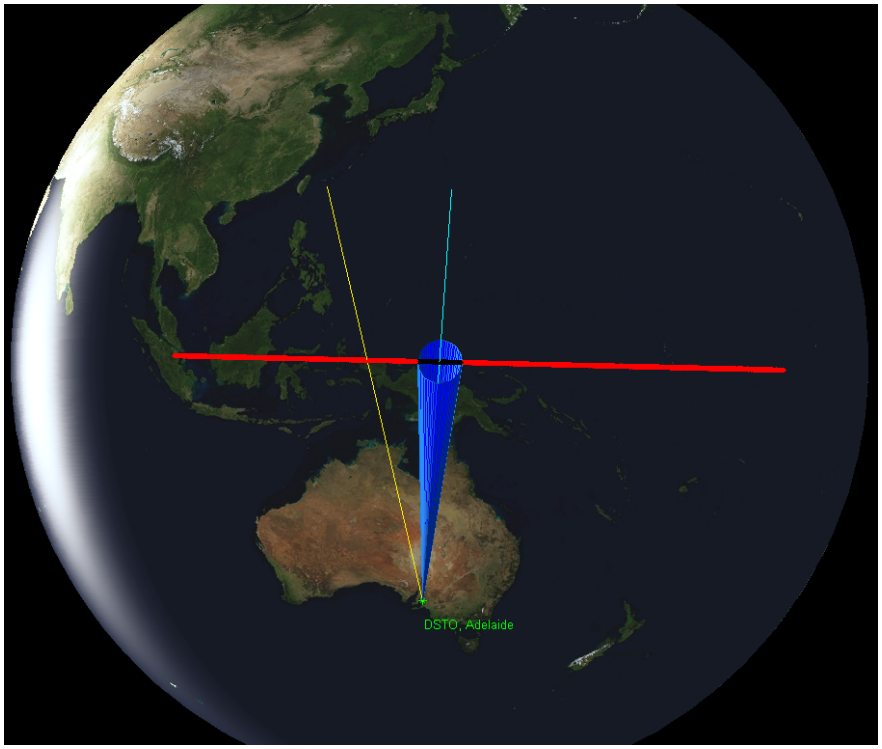

Figure 7: A constrained IOD particle representation of an RSO's state error distribution that is being searched for the RSO, by a sensor performing dynamic steering. The image depicts the sensor's FOV as a blue cone extending from the sensor site in Adelaide to GEO. The particle representation is comprised of red and black particles indicating non-zero and zero weight respectively. The light-blue line coincides with the sensor's boresight and orange line indicates where the sensor's boresight should point to directly target the RSO.

simulations. In general, the number of observations necessary to reacquire Beidou G1 increased with the delay between imaging the satellite and beginning reacquisition. This is not unexpected as the length of the particle distribution, as seen in Fig. 7, was observed to spread along the GEO-belt with increasing delay. The standard deviation of the positions of particles was observed to spread along GEO orbit at a rate of $1.0^\circ/\mathtt{day}$. Thus the constant FOV of the sensor was faced with an increasingly large region of high-probability in which to search for the target, with each passing day.

After a delay of approximately 25 days, the particle distribution was observed to propagate below the sensor's simulated 15° elevation constraint. Consequently, during simulations involving delays of greater than or equal to 25 days, there was more than an insignificant likelihood that the target could have resided at elevations the sensor was unable to image. As SPARSE had been made aware of the sensor's pointing constraints via an appropriate sensor aiming vector $\mathbf{\Psi}$, SPARSE would only search within regions at elevations greater than 15 degrees.

6. DISCUSSION

Fig. 8 displays a prominent spike in the number of observations necessary for reacquisition at 19 days delay. This particular simulation was consequently investigated in greater detail. The cause of the spike appears to be a result of the sensor making two independent observations, slightly to each side of the target, leaving a small, isolated and unobserved region containing the target. As the sensor was seeking pointing angles with the greatest probability of detection, the isolated region did not rate highly enough to be searched until a significant portion of the remaining distribution had been observed. This behaviour is a new phenomenon that has not previously been seen or reported when using the maximum weight steering method (1). It is believed this new behaviour may be attributable to the uniform sampling of the CAR, resulting in a distribution of particles that is much more uniform than has previously been evaluated. In the absence of global and local peaks in the distribution, the pointing angles chosen by SPARSE appear more arbitrary as it moves about, searching the distribution. The use of a uniform distribution

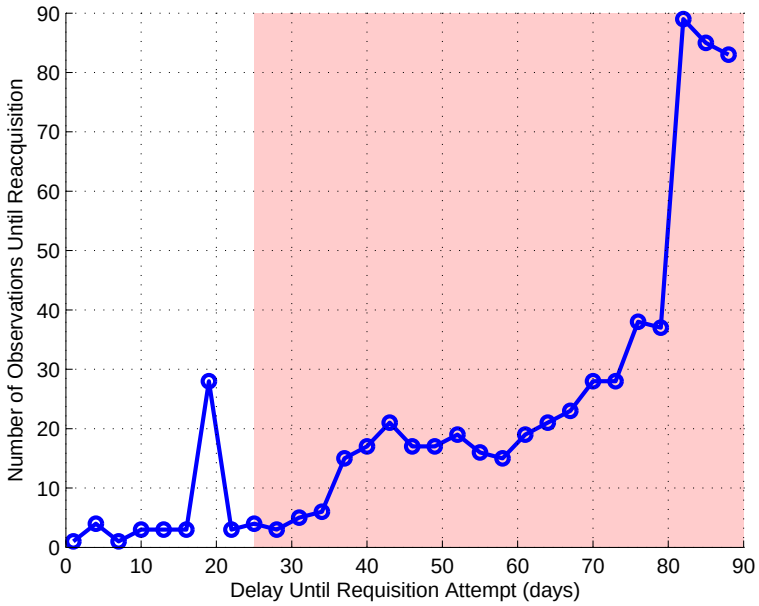

Figure 8: A plot of the number of observations required to locate the target relative to the age of the image used to initialise the search. The red region indicates the delays in which the particle distribution propagated beyond the steering constraints of the sensor.

was nonetheless a naïve first choice and it is probable that the process would benefit from additional consideration regarding the likelihood of range and range-rates across the CAR. This aspect, along with alternative, more suited search methodologies, will therefore be a point of future research.

The results of this initial investigation are nevertheless encouraging and motivate further attempts at field trials. In all test cases, the target was reacquired in spite of a lack of precise information regarding the target's range and range-rate, and the delay between obtaining imagery and attempting reacquisition. The proposed process enabled the reacquisition of a simulated UCT as much as 3 months after it was briefly imaged. Furthermore, if the delay between imaging and reacquisition was less than 30 days, the target, in all but one case, was reacquired in less than 5 observations.

As a preliminary study, it was desirable to learn if objects can be reacquired via this approach whilst neglecting the significant role effective data association will almost certainly play. Clearly, this approach could result in further detections of UCTs and will likely require the incorporation of real-time data-association when objects are detected.

REFERENCES

[1] National Research Council of the National Academies, *Continuing Kepler's Quest: Assessing Air Force Space Command's Astrodynamics Standards*. The National Academies Press, 2012.

[2] M. Wasson, "Space situational awareness in the Joint Space Operations Center," in *Air Force Air and Space Operations Center (614th) Peterson AFB Co.*, 2011.

[3] T. Kelecy and M. Jah, "Analysis of orbit prediction sensitivity to thermal emissions acceleration modeling for high area-to-mass ratio (HAMR) objects," in *Proc. the Advanced Maui Optical and Space Surveillance Technologies Conf., (AMOS)*, 2009.

[4] D. F. Woods, R. Y. Shah, J. A. Johnson, A. Szabo, E. C. Pearce, R. L. Lambour, and W. J. Faccenda, "Space surveillance telescope: focus and alignment of a three mirror telescope," *Optical Engineering*, vol. 52, no. 5, pp. 053 604–053 604, 2013.

[5] N. Singh, J. T. Horwood, J. M. Aristoff, A. B. Poore, C. Sheaff, and M. K. Jah, "Multiple hypothesis tracking (mht) for space surveillance: Results and simulation studies," DTIC Document, Tech. Rep., 2013.

[6] M. J. Holzinger, K. K. Luu, C. Sabol, and K. Hill, "Probabilistic tracklet characterization and prioritization using admissible regions," in *Proceedings of the 2014 Advanced Maui Optical and Space Surveillance Technologies Conference, Wailea, Maui, Hawaii*, 2014.

[7] T. A. Hobson and I. V. L. Clarkson, "A Particle-based Search Strategy for Improved Space Situational Awareness," 3-6 Nov 2013, accepted in Asilomar Conf. on Signals Systems, and Computers.

[8] ——, "An experimental implementation of a particle-based dynamic sensor steering method for tracking and searching for space objects," 4-9 May 2014, accepted in proceedings of IEEE International Conference on Acoustics, Speech and Signal Processing (ICASSP).

[9] T. A. Hobson, "Sensor management for enhanced catalogue maintenance of resident space objects," Ph.D. thesis, The University of Queensland, 2015.

[10] W. Koch, "On negativeinformation in tracking and sensor data fusion: Discussion of selected examples," in *Proceedings of the Seventh International Conference on Information Fusion*, vol. 1. IEEE Publ. Piscataway, NJ, 2004, pp. 91–98.

[11] J. Hoffman, M. Spranger, D. Gohring, and M. Jungel, "Making use of what you don't see: Negative information in markov localization," in *Intelligent Robots and Systems, 2005.(IROS 2005). 2005 IEEE/RSJ International Conference on.* IEEE, 2005, pp. 2947–2952.

[12] K. Poole, J. Woloschek, E. Murphy, J. Lefever, and J. Breslin, "Strategies for optimizing geo debris search," in *The Advanced Maui Optical and Space Surveillance Technologies Conference*, vol. 1, 2006, p. 66.

[13] K. J. DeMars, M. K. Jah, and P. W. Schumacher Jr, "Initial orbit determination using short-arc angle and angle rate data," *Aerospace and Electronic Systems, IEEE Transactions on*, vol. 48, no. 3, pp. 2628–2637, 2012.

[14] S. Haykin, *Adaptive Filter Theory*, 3rd ed. Upper Saddle River, New Jersey: Prentice-Hall, 1996.

[15] B. Ristic, S. Arulampalam, and N. Gordon, *Beyond the Kalman Filter.* Artech House, 2004.

[16] K. J. DeMars and M. K. Jah, "Probabilistic initial orbit determination using gaussian mixture models," *Journal of Guidance, Control, and Dynamics*, vol. 36, no. 5, pp. 1324–1335, 2013.

[17] T. A. Hobson and I. V. L. Clarkson, "GPU-based space situational awareness simulation utilising parallelism for enhanced multi-sensor management," in *Proc. the Advanced Maui Optical and Space Surveillance Technologies Conf., (AMOS)*, 2012.

[18] Y. Bar-Shalom, X. R. Li, and T. Kirubarajan, *Estimation with applications to tracking and navigation: theory algorithms and software.* John Wiley & Sons, 2004.

[19] D. A. Vallado, P. Crawford, R. Hujsak, and T. S. Kelso, "Revisiting spacetrack report #3," Aug 2006.